

Vector polarizability of an atomic state induced by a linearly polarized vortex beam: External control of magic, tune-out wavelengths, and heteronuclear spin oscillations

Anal Bhowmik ^{1,2,*}, Narendra Nath Dutta ³, and Sonjoy Majumder ^{4,†}

¹*Haifa Research Center for Theoretical Physics and Astrophysics, University of Haifa, Haifa 3498838, Israel*

²*Department of Mathematics, University of Haifa, Haifa 3498838, Israel*

³*Department of Chemical Sciences, Indian Institute of Science Education and Research Mohali, Punjab-140306, India*

⁴*Department of Physics, Indian Institute of Technology Kharagpur, Kharagpur-721302, India*

 (Received 2 October 2019; revised 24 November 2020; accepted 30 November 2020; published 21 December 2020)

Experiments with vortex beams have shown a surge of interest in controlling cold atoms. Most of the controlling protocols are dominated by circularly polarized light due to its ability to induce vector polarization at atoms, which is impossible for paraxial linearly polarized light. Here we develop a theory for frequency dependent polarizability of an atomic state interacting with a focused linearly polarized vortex beam. The naturally induced spin-orbit coupling in this type of linearly polarized beam produces vector component of the valence polarizability to an atomic state, obeying the total angular-momentum conservation of the beam. The theory is employed on $^{87}\text{Sr}^+$ to accurately calculate the magic wavelengths for the clock transitions and tune-out wavelengths for the clock states using the relativistic coupled-cluster method. The induced vector component in the dynamic polarizability due to the linearly polarized focused vortex beam promotes a fictitious magnetic field to the atomic state. We demonstrate that this fictitious magnetic field, depending on the focusing angle and orbital angular momentum of the beam, improves the flexibility of the coherent heteronuclear spin oscillations in a spin-1 mixture of ^{87}Rb and ^{23}Na atoms.

DOI: [10.1103/PhysRevA.102.063116](https://doi.org/10.1103/PhysRevA.102.063116)

I. INTRODUCTION

In recent years, laser trapping and cooling of neutral atoms have attracted significant attention from experimentalists and become an established technique in high-precision spectroscopic measurements [1–3]. Along with neutral atoms, optical dipole trappings of ions have recently bolstered interest in ultracold physics [4–7]. However, the mechanism of the trapping by optical means inevitably produces Stark shifts in the atomic energy levels and influences the fidelity of the precision measurements. Magic wavelengths are the unique wavelengths of the external laser beam for which the differential AC-Stark shift of an atomic transition effectively vanishes. Therefore, the impediment in precise spectroscopic measurements can be eliminated almost entirely if the atoms are confined at the predetermined magic wavelengths of the laser beam. The light at magic wavelengths have significant applications in atom optics, such as atomic interferometers [8], atomic clocks [9–11], and atomic magnetometers [12].

Determinations of magic wavelengths for an atomic transition depend mainly on how accurately the frequency-dependent valence polarizability (POL) values of the atomic Zeeman sublevels are calculated. The valence POL consists of three components, scalar POL (α_V^0), vector POL (α_V^1), and tensor POL (α_V^2) [13–16]. In general, POL is defined in

terms of an off-resonant electric-dipole interaction between the atom and its trapping light. The vector POL, which yields the energy shift among the Zeeman sublevels, arises usually due to a circularly polarized light [13,17,18]. It is one of the non-magnetic-field sources to remove the Zeeman degeneracy and becomes very significant in the evaluation of magic wavelengths for cases such as “knob” to adjust an optical trap [19].

In this work, we theoretically develop and demonstrate that a linearly polarized focused vortex (LP-FV) beam can naturally produce the vector part of the dynamic POL when it interacts with cold atoms or ions. The vector part is certainly not a component of dynamic POL for a linearly polarized Gaussian or paraxial vortex beam. The distinctive feature of the vortex beam is that, in addition to the spin angular momentum associated with the polarization, it has orbital angular momentum (OAM) which arises due to the helical phase front of the beam [20–30]. We find that the origin of the vector POL comes from the prolific artifacts of the spin-orbit coupling of the LP-FV beam satisfying conservation of the total angular momentum of the beam during the interaction process. Also, this vector POL creates a fictitious magnetic field [31] when it interacts with an atomic system. This fictitious magnetic field interrogates, manipulates, and traps an atom or ion independently [32] or in conjunction with the real magnetic field [33]. Furthermore, this fabricated field provides a unique opportunity for exploring spin dynamics in the form of coherent spin oscillations [34–37] in the ultracold spinor quantum gas. This has been the subject of intensive theoretical and experimental research due to its high controllability [38].

*abhowmik@campus.haifa.ac.il

†sonjoym@phy.iitkgp.ernet.in

The primary objective of the present work is to visualize the effect of vector POL, which originates due to the spin-orbit coupling of the LP-FV beam, in the clock transitions and clock states. We apply our theory to calculate the dynamic POL values of the fine-structure states $5S_{\frac{1}{2}}$, $4D_{\frac{3}{2}}$, and $4D_{\frac{5}{2}}$ of $^{87}\text{Sr}^+$. Singly ionized strontium is an excellent candidate for an optical frequency standard, quantum information, and quantum storage [39,40]. As the spin-orbit coupling of LP-FV beam varies with the choice of OAM and focusing angle of the lens, we quantitatively show the effects of these parameters on the magic wavelengths for $5S_{\frac{1}{2}} \rightarrow 4D_{\frac{3}{2}, \frac{5}{2}}$ transitions and tune-out wavelengths (where the dynamic POL value becomes zero [41,42]). These quantifications will be important for the experimentalists to choose the parameters of the vortex beams used for trapping [19,32]. To manifest the impact of the vector POL, we compare the calculated magic and tune-out wavelengths induced from the LP-FV beam with the corresponding wavelengths induced from a linearly polarized Gaussian beam. Moreover, as an important application, we investigate how the fictitious magnetic field, originated from the vector POL, can control the coherent heteronuclear spin oscillations in a spin-1 mixture of ^{87}Rb and ^{23}Na atoms with influences from both linear and quadratic Zeeman shifts.

II. THEORY

According to time-independent second-order perturbation theory [43], the AC-Stark shift of an atomic state in an external oscillating electric field $\mathcal{E}(\omega)$ is expressed by $\Delta F(\omega) = -\frac{1}{2}\alpha^T(\omega)\mathcal{E}^2$, where $\alpha^T(\omega)$ is the total dynamic POL of the atomic state at frequency ω and \mathcal{E} is the magnitude of the external electric field. For a single-valence atom with a valence electron in the ν th orbital, the total dynamic POL can be written as $\alpha^T(\omega) = \alpha^C(\omega) + \alpha^{VC}(\omega) + \alpha^V(\omega)$. Here $\alpha^C(\omega)$ is the frequency-dependent core POL of the ionic core obtained by removing the valence electron. $\alpha^{VC}(\omega)$ gives a correction [44] to the core POL due to the presence of the valence electron and is considered as ω independent in the present work. $\alpha^V(\omega)$ is the valence POL of the single-valence state. α^C and α^{VC} provide small contributions to α^T compared with α^V , and they are computed approximately by using lower-order many-body perturbation theory [43,45,46].

Now we evaluate $\alpha^V(\omega)$ in the presence of an external LP-FV beam. As a Laguerre-Gaussian (LG) beam is a well-established example of a vortex beam, initially, we assume a paraxial form of a linearly polarized coherent LG beam without any off-axis node and that propagates along the z axis. The field is expressed as [24] $\mathcal{E}_i(\rho, \phi, z, t) = \mathcal{E}_i(t)(\sqrt{2\rho/w_0})^{|l|} e^{i(l\phi + k_0z)} \hat{\mathbf{x}}$. Here k_0 is the wave number of the free space, w_0 is the waist-size, and l is OAM of the beam. We consider that this paraxial LG beam is focused by passing through an objective (lens) with a high numerical aperture (NA) [25]. Then this focused LG beam interacts with a cold atom or ion whose de Broglie wavelength is large enough to experience the intensity variation of this beam. To take a full advantage of the high NA of the lens, we assume that w_0 overfills the entrance aperture radius. According to Kirchhoff's approximation in diffraction theory [47,48], the consequent components of the spin-orbit coupled LP-FV beam can be

expressed as

$$\begin{aligned} \mathcal{E}(\rho, \phi, z, t) &= \begin{bmatrix} \mathcal{E}_x \\ \mathcal{E}_y \\ \mathcal{E}_z \end{bmatrix} = (-i)^{l+1} \mathcal{E}_0 e^{i(l\phi - \omega t)} \\ &\times \begin{bmatrix} u_l(\rho, z) + u_{l+2}(\rho, z)e^{2i\phi} + u_{l-2}(\rho, z)e^{-2i\phi} \\ -i[u_{l+2}(\rho, z)e^{2i\phi} - u_{l-2}(\rho, z)e^{-2i\phi}] \\ -i[u_{l+1}(\rho, z)e^{i\phi} - u_{l-1}(\rho, z)e^{-i\phi}] \end{bmatrix}. \end{aligned} \quad (2.1)$$

Here \mathcal{E}_x , \mathcal{E}_y , and \mathcal{E}_z are the x , y , and z components of the electric field, respectively. The amplitude of the focused electric field is $\mathcal{E}_0 = \frac{\pi f}{\lambda} T \mathcal{E}_i$, where \mathcal{E}_i is the amplitude of the incident electric field, T is the transmission coefficient of the objective, and f is its focal length related to ρ by $\rho = f \sin \theta$ (Abbe sine condition). The coefficients u_{l+m} , where m takes the values 0, ± 1 , and ± 2 in the above expression depend on the focusing angle of NA (ϑ_m) following the relation [49] $u_{l+m}(\rho, z) = \int_0^{\vartheta_m} d\vartheta (\frac{\sqrt{2\rho}}{w_0})^{|l|} \sin \vartheta \sqrt{\cos \vartheta} g_{|m|}(\vartheta) J_{l+m}(k\rho \sin \vartheta) e^{ikz \cos \vartheta}$. Here $J_{l+m}(k\rho \sin \vartheta)$ represents the cylindrical Bessel function, and $k = \mu k_0$ with μ as the refractive index of the lens medium. $g_{|m|}(\vartheta)$ are the angular functions with $g_0(\vartheta) = 1 + \cos \vartheta$, $g_1(\vartheta) = \sin \vartheta$, and $g_2(\vartheta) = 1 - \cos \vartheta$.

Now let us discuss Eq. (2.1) in detail. Linearly polarized light can be considered as the superposition of left ($\beta = +1$) and right ($\beta = -1$) circularly polarized beams. Because of the focusing and the diffraction from the edges of the aperture, each circularly polarized light ($\beta = \pm 1$) can be decomposed into three sets of local polarizations (± 1 , ∓ 1 , and polarization along the z axis) [25]. Among these three sets of local polarizations, the first set has equal amplitude (u_l) for ± 1 local polarizations. Therefore, after passing through the focusing lens, the superposition of these local polarizations results in a linearly polarized beam with an OAM similar to the OAM of the incident beam. However, in the case of the second set, different field amplitudes, u_{l+2} and u_{l-2} , are generated with two different local polarizations (-1 and $+1$, respectively) and topological charges ($l+2$ and $l-2$, respectively, to conserve total angular momentum) after passing through the lens. Therefore, the field gains two opposite circular polarizations with different amplitudes and creates the vector part of the valence POL in interaction with an atom or ion. The third set yields u_{l+1} and u_{l-1} fields with topological charges, $l+1$ and $l-1$, respectively. However, both these fields are polarized along the z direction, which is another interesting manifestation of a focusing beam. Nevertheless, using LP-FV beam presented in Eq. (2.1), $\alpha^V(\omega)$ of the atomic state can be presented by

$$\alpha^V(\omega) = C_0 \alpha_V^0(\omega) + C_1 \alpha_V^1(\omega) + C_2 \alpha_V^2(\omega). \quad (2.2)$$

Here the coefficients C_i s are expressed in the following forms:

$$\begin{aligned} C_0 &= \{u_l\}^2 + \{u_{l+1}\}^2 + \{u_{l-1}\}^2 + 2[\{u_{l+2}\}^2 + \{u_{l-2}\}^2], \\ C_1 &= [2\{u_{l-2}\}^2 - 2\{u_{l+2}\}^2] \left(\frac{M_{J_V}}{2J_V} \right), \\ C_2 &= [\{u_l\}^2 - \{u_{l+1}\}^2 - \{u_{l-1}\}^2 + 2\{u_{l+2}\}^2 + 2\{u_{l-2}\}^2] \\ &\quad \times [(3M_{J_V}^2 - J_V(J_V + 1))/(2J_V(2J_V - 1))], \end{aligned} \quad (2.3)$$

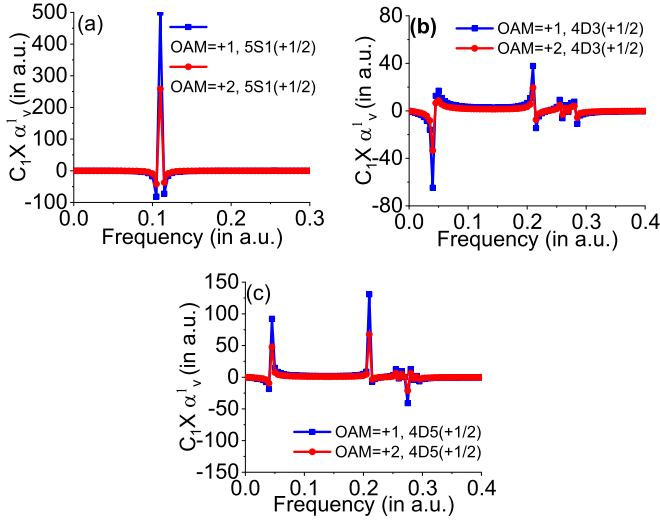


FIG. 1. Frequency-dependent total vector POL ($C_1\alpha_V^1$) of $5S_{1/2}(+1/2)$ and $4D_{3/2,5/2}(+1/2)$ states for LP-FV beam with OAM = +1 and +2 at focusing angle 60° .

where J_V and M_{J_V} are the total angular momentum and its magnetic component for the single-valence atomic state $|\Phi_V\rangle$. The mathematical expressions of the scalar, vector, tensor, and consequently the valence POL at the fine- and hyperfine-structure levels are presented in the Appendix. The calculation of $\alpha^V(\omega)$ [17,43] of an atomic state directly depends on different combinations of the integrals u_{l+m} . These integrals can be altered with the various choices of the topological charges of the incident LG beam and the NA of the objective. As a consequence, the total POL values of the atomic states and the magic wavelengths for the transitions among them can be tuned externally by using different parameters of the beam.

III. RESULTS AND DISCUSSIONS

As the electron correlation most significantly affects the $\alpha^V(\omega)$ part of the dynamic POL due to the loosely bound valence electron, the accurate estimates of the scalar, vector, and tensor components of $\alpha^V(\omega)$ for the different states require correlation-exhaustive many-body calculations [50–58] with a sophisticated numerical approach (see Appendix for details of the computations). To have a quantitative analysis of the effect of OAM of LP-FV beam on the total vector POL [$C_1\alpha_V^1(\omega)$] of an atomic state, we show variations of $C_1\alpha_V^1(\omega)$ with frequency for $5S_{1/2}(+1/2)$ and $4D_{3/2,5/2}(+1/2)$ states of $^{87}\text{Sr}^+$ in Fig. 1 [$M_J = -\frac{1}{2}$ provides the opposite sign of $C_1\alpha_V^1(\omega)$]. The fine-structure states $5S_{1/2}$, $4D_{3/2}$, and $4D_{5/2}$ are indicated by 5S1, 4D3, and 4D5, respectively in this figure and the next two figures of this paper. Here LP-FV beam has either OAM = +1 or +2 with focusing angle of 60° . Although the effect of variation of focusing angle to $C_1\alpha_V^1(\omega)$ is marginal, it is significant to the total scalar and tensor POL values, and consequently to the total POL values. The peak values of $C_1\alpha_V^1(\omega)$ occur at resonance frequencies: 0.11 a.u. for $5S_{1/2}$ state; around 0.045 a.u. and 0.21 a.u. for $4D_{3/2}$ and $4D_{5/2}$ states, respectively. However, many small-scale structures in

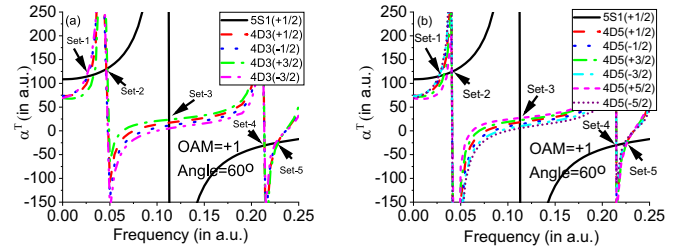


FIG. 2. Frequency-dependent α^T of $5S_{1/2}$ and $4D_{3/2}$ and $4D_{5/2}$ states. LP-FV beam is focused at 60° with OAM = +1. The values inside the parentheses indicate the magnetic components. The corresponding wavelengths at the intersections of the polarizability curves of $5S_{1/2}$, $4D_{3/2}$, and $4D_{5/2}$ states are the magic wavelengths for the clock transitions $5S_{1/2}-4D_{3/2}$ and $5S_{1/2}-4D_{5/2}$. For both these clock transitions, five sets (Set 1 to Set 5) of magic wavelengths are found.

the $C_1\alpha_V^1(\omega)$ profiles of the $4D_{3/2}$ and $4D_{5/2}$ states appear due to the multiple resonance transitions around 0.25 to 0.30 a.u.

It can be seen from the graphs that OAM = +1 always produces a higher peak value of $C_1\alpha_V^1(\omega)$ compared with OAM = +2. This is because of the stronger spin-orbit coupling for OAM = +1 compared with OAM = +2. Also, the magnitude of the peak value of $C_1\alpha_V^1(\omega)$ is higher for larger M_J for a fixed value of J , which is obvious from the expression of C_1 .

Figure 2 displays profiles of α^T for $5S_{1/2}$ and $4D_{3/2}$ and $4D_{5/2}$ states of $^{87}\text{Sr}^+$ at 60° focusing angle for LP-FV beam with OAM = +1. However, it should be mentioned that focusing angle does affect α^T values at various frequencies of the beam. Figure 2 shows a number of intersection points between α^T profiles of the multiplets of $5S_{1/2}$, $4D_{3/2}$, and $4D_{5/2}$ states. These intersection points indicate the magic wavelengths at which the differential AC-Stark shift of the associated clock transition states vanishes. We observe five sets (Set 1 to Set 5) of magic wavelengths for $5S_{1/2} \rightarrow 4D_{3/2}$, $4D_{5/2}$ clock transitions within the frequency span (from the near-infrared to the ultraviolet regions) as shown in the figures (see Appendix). This is true for all the magnetic sublevels involved in the transitions. However, the infrared magic wavelengths (fall under Set 1 and Set 2) are the most important to trap $^{87}\text{Sr}^+$ due to relatively large α^T values and support the red-detuned trapping scheme useful for frequency-standard experiments. We find that the magic wavelengths for the clock transitions at Set 1 are maximally affected by the spin-orbit coupling of the beam. For the $5S_{1/2} \rightarrow 4D_{5/2}(+3/2)$ transition, the magic wavelength at Set 1 is 1793.83 nm for either linearly polarized paraxial LG beam or Gaussian beam. The results are the same because the OAM of the paraxial light does not affect the electronic motion of a cold atom or ion (which is below its recoil limit) at the dipole transition level [17,24]. However, we observe that, for OAM = +1 and +2 of the LP-FV beam, the magic wavelengths of the $5S_{1/2} \rightarrow 4D_{3/2}(+3/2)$ transition at Set 1 can be varied up to -20% and -15% , respectively, compared with the corresponding magic wavelength of a Gaussian beam.

Figure 3 illustrates wavelength dependence on α^T for the clock transition state $4D_{3/2}$ of $^{87}\text{Sr}^+$ due to the external field of LP-FV beam with OAM = +1 and +2, focused at an angle of

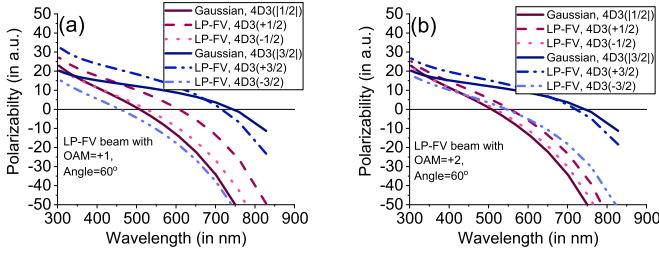


FIG. 3. Variation of α^T (in a.u.) with wavelength (in nm) for all the magnetic components of the state $4D_{3/2}$ for the LP-FV beam focused at 60° [with (a) $OAM = +1$ and (b) $OAM = +2$] and paraxial Gaussian beam are presented. Wavelengths at which the curves intersect the zero-polarizability axis are the tune-out wavelengths.

60° , and linearly polarized paraxial Gaussian beam. Because the beam is linearly polarized, the vector component does not arise in α^T for the Gaussian beam. Therefore, the tune-out wavelengths for the $4D_{3/2}$ ($M_J = \pm 1/2$) and $4D_{3/2}$ ($M_J = \pm 3/2$) states are degenerate with respect to the sign of M_J and their values are 507.83 and 744.12 nm, respectively. These degeneracies are lifted for the LP-FV beam. This leads to splitting of the tune-out wavelengths for the oppositely signed M_J -levels with respect to the corresponding tune-out wavelengths for the linearly polarized Gaussian beam. The figure shows that nonzero OAM of the LP-FV beam causes redshifting and blueshifting of the tune-out wavelengths with respect to the tune-out wavelengths of the Gaussian beam for $M_J = |\frac{1}{2}|$ and $M_J = |\frac{3}{2}|$, respectively. The comparison of Figs. 3(a) and 3(b) reveals that the separation between the tune-out wavelengths corresponding to $+M_J$ and $-M_J$ of a particular value of M_J decreases with the increasing OAM of the beam. This also indicates the decreasing strength of the spin-orbit coupling with the increasing OAM of the LP-FV beam.

We also gauge the effect of the vector POL arising from LP-FV beam by considering a heteronuclear spin-1 mixture of ^{87}Rb and ^{23}Na atoms with spin states $|M_{F_{V1}}\rangle$ and $|M_{F_{V2}}\rangle$, respectively, of $F_{V1} = F_{V2} = 1$ hyperfine levels of their respective ground states $5S_{1/2}$ and $3S_{1/2}$. Here, we show how their coherent spin oscillations can be controlled by the fictitious magnetic field generated from the vector POL due to the LP-FV beam. We calculate the total magnetic energy $E^{|M_{F_{V1}}, M_{F_{V2}}\rangle}(B)$ (from the Breit-Rabi formula [59]) associated with the $|M_{F_{V1}}, M_{F_{V2}}\rangle$ state, where B is the externally applied magnetic field. In this example, we start with $|0, 0\rangle$ mixture of ^{87}Rb and ^{23}Na atoms. Therefore, we have only two types of spin-changing transition process at the $F_V = 1$ level conserving the total magnetization: $|0, 0\rangle \leftrightarrow |-1, 1\rangle$ and $|0, 0\rangle \leftrightarrow |1, -1\rangle$. In the presence of a laser beam, the magnitudes of the frequency-dependent Stark-shifts for both the atoms largely depend on the positions of the D -line transitions, which are close to 590 and 790 nm for the ^{23}Na and ^{87}Rb atoms, respectively. Therefore, if a light beam of wavelength nearly 790 nm is used, it can make the Stark shift essentially species-selective for ^{87}Rb , but mostly transparent for ^{23}Na . The dynamic polarizability for the state $|5S_{1/2}, F_V = 1, M_{F_V} = 0, \pm 1\rangle$ of ^{87}Rb is depicted in Fig. 4(a) for 786–794 nm. Here a LP-FV beam with intensity 10 W/cm^2 and both $OAM = +1, +2$ are employed to selectively dress

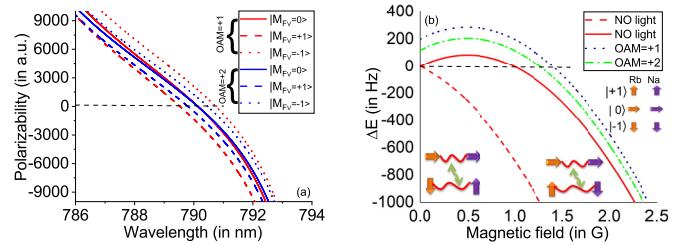


FIG. 4. (a) Variation of α^T (in a.u.) with wavelength (in nm) for the ground state of the ^{87}Rb at the hyperfine level $F_V = 1$ for the LP-FV beam focused at 60° . (b) Magnetic energy diagram for the two heteronuclear spin-oscillation processes without light shift: $|0, 0\rangle \leftrightarrow |-1, 1\rangle$ (red dashed) and $|0, 0\rangle \leftrightarrow |1, -1\rangle$ (red solid). Blue dot and green dash-dot curves are magnetic energy variations with $OAM = +1$ and $+2$, respectively, for $|0, 0\rangle \leftrightarrow |1, -1\rangle$. The intensity of the LP-FV beam is assumed to be 10 W/m^2 .

the energy levels of ^{87}Rb near 790.14 nm wavelength, which is the tune-out wavelength for the $M_{F_V} = 0$ state. The figure shows that the Stark shift for $M_{F_V} = \pm 1$ is larger for $OAM = +1$ compared with $OAM = +2$ at the wavelength 790.14 nm.

Without the LP-FV beam, the total Zeeman energy difference of the process $|0, 0\rangle \leftrightarrow |-1, 1\rangle$ is indicated by $\Delta E^-(B) = E^{|0,0\rangle} - E^{|-1,1\rangle}$ and of the process $|0, 0\rangle \leftrightarrow |1, -1\rangle$ is indicated by $\Delta E^+(B) = E^{|0,0\rangle} - E^{|1,-1\rangle}$. These Zeeman energy differences of the heteronuclear spin-oscillations include contributions of both the linear and quadratic Zeeman shifts [60]. Since the heteronuclear spin oscillation can only occur near $\Delta E^\pm(B) = 0$ [61], Fig. 4(b) suggests that only the oscillation $|0, 0\rangle \leftrightarrow |1, -1\rangle$ is possible at the magnetic field 0.99 G. The other oscillation, $|0, 0\rangle \leftrightarrow |-1, 1\rangle$, is strongly suppressed at this magnetic field. Now, taking into account the light shift by the LP-FV beam on ^{87}Rb atoms at the wavelength of 790.14 nm, the total Zeeman energy difference of the allowed process is modified to $\Delta E^+(B) = (E^{|0,0\rangle} - E^{|1,-1\rangle}) + [\delta E_l(M_{F_V} = 0) - \delta E_l(M_{F_V} = 1)]$, where δE_l is the light shift. In Fig. 4(b), we find that $\Delta E^+(B)$ becomes zero at the magnetic fields 1.40 and 1.26 G for $OAM = +1$ and $+2$, respectively, of the LP-FV beam. Therefore, the external magnetic field that is required for $|0, 0\rangle \leftrightarrow |1, -1\rangle$ transition with $\Delta E^+(B) = 0$ to take place is changed significantly due to the presence of the LP-FV beam, which accounts for the fictitious magnetic field generated by the vector polarizability. This is purely a manifestation of the vector light shift that arises from the spin-orbit coupling of the beam. Also, the spin oscillation process of the heteronuclear spin-1 mixture of ^{87}Rb and ^{23}Na can be controlled externally by changing the focusing angle and OAM of LP-FV beam. This process will be very useful for recent experiments using spherical-quadrupole magnetic traps [62].

IV. CONCLUSION

In summary, we have developed a theoretical formalism to calculate the dynamic POL of an atomic state in the external field of a LP-FV beam. We have demonstrated how the OAM and focusing angle of the beam induce the spin-orbit coupling in the beam, which in turn produces vector polarizability in the

atomic state even for linearly polarized light. The fine tuning of magic wavelengths for the clock transitions $5S_{\frac{1}{2}} \rightarrow 4D_{\frac{3}{2}, \frac{5}{2}}$ of $^{87}\text{Sr}^+$ ion are demonstrated by controlling the OAM and focusing parameters of the LP-FV beam (details are in the Appendix). The vector POL values presented in this paper can be verified experimentally by stimulated Raman spectroscopy [63] or by measuring the tune-out wavelengths for the magnetic sublevels of identical multiplets [64,65]. Moreover, we develop a controlling mechanism of heteronuclear spin oscillations of spin-1 mixture of ^{87}Rb and ^{23}Na atoms with the fictitious magnetic field generated by the LP-FV beam. This mechanism can be used to tune the heteronuclear spin dynamics [66] and generate entanglement between distinguishable atoms [67]. We believe that the present theoretical development will give an additional flexibility in the spin-changing interaction process of other multispecies spinor condensates.

ACKNOWLEDGMENT

A.B. acknowledges Arghya Das for helpful discussions.

APPENDIX

In Sec. A, we present a brief mathematical description of the scalar, vector, and tensor polarizabilities of a single-valence atomic state at the fine-structure and hyperfine levels. In Sec. B, we show the numerical procedure to calculate the dynamic polarizabilities of $^{87}\text{Sr}^+$ and ^{87}Rb . In this section, we also include the details of the Zeeman energy difference that leads the spin oscillation processes of the spin-1 mixture ^{87}Rb and ^{23}Na atoms. In Sec. C, we tabulate a list of magic wavelengths and the corresponding vector and total polarizabilities for the clock transitions $5S_{\frac{1}{2}} \rightarrow 4D_{\frac{3}{2}, \frac{5}{2}}$ of $^{87}\text{Sr}^+$ ion.

1. Scalar, vector, and tensor polarizabilities at the fine-structure and hyperfine levels

$\alpha_V^0(\omega)$, $\alpha_V^1(\omega)$, and $\alpha_V^2(\omega)$ are the scalar, vector, and tensor components, respectively, of the dynamic valence polarizability $\alpha^V(\omega)$ at the fine-structure level of the single-valence state Ψ_V . These components are expressed using the sum-over-states approach [13–16,43,44] as follows:

$$\alpha_V^0(\omega) = \frac{2}{3(2J_V + 1)} \sum_N \frac{|\langle \Psi_V || d || \Psi_N \rangle|^2 \times (\epsilon_N - \epsilon_V)}{(E_N - E_V)^2 - \omega^2}, \quad (\text{A1})$$

$$\alpha_V^1(\omega) = -\sqrt{\frac{6J_V}{(J_V + 1)(2J_V + 1)}} \sum_N (-1)^{J_N + J_V} \times \begin{Bmatrix} J_V & 1 & J_V \\ 1 & J_N & 1 \end{Bmatrix} \frac{|\langle \Psi_V || d || \Psi_N \rangle|^2 \times 2\omega}{(E_N - E_V)^2 - \omega^2}, \quad (\text{A2})$$

$$\alpha_V^2(\omega) = 4\sqrt{\frac{5J_V(2J_V - 1)}{6(J_V + 1)(2J_V + 1)(2J_V + 3)}} \sum_N (-1)^{J_N + J_V} \times \begin{Bmatrix} J_V & 1 & J_N \\ 1 & J_V & 2 \end{Bmatrix} \frac{|\langle \Psi_V || d || \Psi_N \rangle|^2 \times (\epsilon_N - \epsilon_V)}{(E_N - E_V)^2 - \omega^2}. \quad (\text{A3})$$

Here J_V is the total angular momentum and E_V is the ionization potential of Ψ_V . $\langle \Psi_V || d || \Psi_N \rangle$ is the reduced matrix element of the electric-dipole operator.

At a hyperfine level F_V with nuclear spin I , the scalar component $\alpha_{VF}^0(\omega)$ of the valence polarizability is equal to $\alpha_V^0(\omega)$. This is because of the second-order scalar energy shift does not depend on any hyperfine quantum number [68]. But the hyperfine-induced vector $\alpha_{VF}^{(1)}(\omega)$ and tensor $\alpha_{VF}^{(2)}(\omega)$ components have different angular-momentum factors to be multiplied with the above expressions for $\alpha_V^1(\omega)$ and $\alpha_V^2(\omega)$, respectively [18,68,69]:

$$\alpha_{VF}^{(1)}(\omega) = (-1)^{J_V + F_V + I + 1} \begin{Bmatrix} F_V & J_V & I \\ J_V & F_V & 1 \end{Bmatrix} \times \sqrt{\frac{F_V(2F_V + 1)(2J_V + 1)(J_V + 1)}{J_V(F_V + 1)}} \alpha_V^1(\omega) \quad (\text{A4})$$

and

$$\alpha_{VF}^{(2)}(\omega) = (-1)^{J_V + F_V + I} \begin{Bmatrix} F_V & J_V & I \\ J_V & F_V & 2 \end{Bmatrix} \times \sqrt{\left(\frac{F_V(2F_V - 1)(2F_V + 1)}{(2F_V + 3)(F_V + 1)}\right)} \times \sqrt{\left(\frac{(2J_V + 3)(2J_V + 1)(J_V + 1)}{J_V(2J_V - 1)}\right)} \alpha_V^2(\omega). \quad (\text{A5})$$

The total valence polarizability at the hyperfine level [$\alpha_F^V(\omega)$] takes the form

$$\alpha_F^V(\omega) = C_0 \alpha_{VF}^0(\omega) + C_1 \alpha_{VF}^{(1)}(\omega) + C_2 \alpha_{VF}^{(2)}(\omega), \quad (\text{A6})$$

where C_i are the coefficients mentioned in the main text.

2. Details of numerical procedure

Here, we present the numerical procedure to calculate the dynamic polarizability of an atomic state discussed in the main text. The electron-correlation significantly affects the valence polarizability of an atomic state due to the loosely bound valence electron. Therefore, the precise estimations of the scalar, vector, and tensor components of the valence polarizability for an atomic state require correlation-exhaustive many-body treatments with a sophisticated numerical approach.

Calculation of the dynamic polarizability for $^{87}\text{Sr}^+$

To calculate the valence polarizabilities for $5S_{\frac{1}{2}}$, $4D_{\frac{3}{2}}$, and $4D_{\frac{5}{2}}$ states, we consider all possible non-negligible dipole matrix elements in Eqs. (A1) to (A3). This sets the highest principle quantum number of the running index N , which is considered up to 25. According to the significance of each dipole matrix elements to the summations in the equations, many-body calculations of different orders of correlations are performed with negligible compromise in the accuracy of the polarizability values [17]. The most dominant dipole matrix elements are associated with the intermediate states $5P_{1/2,3/2}$ to $8P_{1/2,3/2}$ and $4F_{5/2,7/2}$ to $6F_{5/2,7/2}$ as Ψ_N , and they are computed using a relativistic coupled-cluster theory having cluster operators containing single, double, and valence triple

TABLE I. Magic wavelengths (in nm) with corresponding polarizabilities (in a.u.) of $^{87}\text{Sr}^+$ for different focusing angles of the linearly polarized vortex beam (with OAM = +1 and +2) for transitions $5S_{\frac{1}{2}}(+1/2) \rightarrow 4D_{\frac{3}{2}}(M_J)$. The values in the parentheses refer vector polarizabilities at the corresponding magic wavelengths. In the parentheses (a, b), “a” and “b” indicate the vector polarizabilities for the $5S_{\frac{1}{2}}(+1/2)$ and $4D_{\frac{3}{2}}(M_J)$ states, respectively, in a.u.

State	λ^{50°	α^{50°	λ^{60°	α^{60°	λ^{70°	α^{70°	
OAM = +1							
$4D_{\frac{3}{2}}(M_J)$	$(+\frac{1}{2})$	1627.26	113.53 (−0.16, −7.20)	1598.71	115.45 (−0.16, −7.81)	1571.15	117.37 (−0.16, −7.27)
		992.67	126.99 (−0.33, 12.91)	981.97	129.94 (−0.34, 13.95)	981.97	132.77 (−0.32, 13.14)
		403.57	17.32 (158.00, 3.10)	403.57	17.32 (156.69, 3.07)	403.57	17.32 (158.72, 2.91)
		213.21	−29.88 (−0.13, −0.93)	213.21	−30.79 (−0.13, −0.84)	213.21	−31.81 (−0.13, −0.24)
		200.01	−24.11 (−0.10, −1.37)	200.45	−25.01 (−0.10, −1.43)	200.45	−26.03 (−0.09, −1.24)
$(-\frac{1}{2})$	1786.80	111.60 (−0.15, 5.20)	1752.44	114.54 (−0.15, 6.21)	1752.44	116.47 (−0.14, 5.52)	
	1003.60	126.99 (−0.33, −12.51)	992.67	129.94 (−0.34, −13.25)	992.67	131.86 (−0.32, −12.93)	
	403.57	10.53 (158.00, −3.10)	403.57	10.53 (156.69, −3.07)	403.57	11.54 (158.72, −2.91)	
	213.21	−29.88 (−0.13, 0.93)	213.21	−30.79 (−0.13, 0.84)	213.21	−31.81 (−0.13, 0.24)	
	200.45	−25.01 (−0.10, 1.47)	200.90	−25.01 (−0.10, 1.43)	201.34	−26.03 (−0.09, 1.64)	
$(+\frac{3}{2})$	1368.27	116.47 (−0.19, −40.15)	1389.13	118.39 (−0.20, −37.93)	1406.28	120.32 (−0.19, −34.55)	
	961.25	128.92 (−0.35, 43.73)	961.25	130.84 (−0.37, 43.90)	961.25	133.79 (−0.34, 42.50)	
	403.57	23.09 (158.00, 9.25)	403.57	23.09 (156.69, 9.26)	403.57	23.09 (158.72, 8.75)	
	213.21	−29.88 (−0.13, −2.78)	212.71	−30.79 (−0.13, −18.52)	213.21	−31.81 (−0.13, −2.64)	
	199.58	−24.11 (−0.10, −4.33)	199.58	−25.01 (−0.10, −5.23)	199.58	−25.01 (−0.08, −3.46)	
$(-\frac{3}{2})$	1815.27	111.60 (−0.15, 15.61)	1815.27	113.53 (−0.21, 15.65)	1815.27	116.47 (−0.13, 14.78)	
	981.97	128.01 (−0.34, −41.81)	992.67	128.92 (−0.34, −40.55)	992.67	131.86 (−0.32, −38.00)	
	403.57	4.75 (158.00, −9.25)	403.57	4.75 (156.69, −9.26)	403.57	5.77 (158.72, −8.75)	
	213.21	−29.88 (−0.13, 2.78)	213.21	−30.79 (−0.13, 2.80)	213.21	−31.81 (−0.13, 2.64)	
	202.14	−25.01 (−0.10, 6.21)	202.14	−26.03 (−0.10, 6.13)	201.79	−26.03 (−0.09, 5.29)	
OAM = +2							
$4D_{\frac{3}{2}}(M_J)$	$(+\frac{1}{2})$	2312.86	103.00 (−0.05, −1.66)	2201.13	104.92 (−0.05, −1.91)	2052.40	107.75 (−0.06, −2.15)
		1047.43	117.37 (−0.15, −5.16)	1035.53	119.30 (−0.16, −1.46)	1035.53	122.24 (−0.16, −1.43)
		405.73	13.47 (115.64, 1.51)	403.57	14.37 (86.72, 1.59)	405.73	14.37 (119.91, 1.56)
		213.21	−27.96 (−0.06, −0.55)	213.21	−28.86 (−0.07, −0.48)	213.21	−28.86 (−0.06, −0.47)
		199.66	−22.18 (−0.05, −0.71)	200.01	−23.09 (−0.05, −0.74)	199.58	−23.09 (−0.05, −0.61)
$(-\frac{1}{2})$	2559.74	101.98 (−0.04, 1.43)	2360.80	104.92 (−0.05, 1.71)	2201.13	107.75 (−0.06, 1.88)	
	1035.53	117.37 (−0.16, 1.38)	1035.53	119.30 (−0.16, 1.46)	1035.53	122.24 (−0.16, 1.43)	
	403.57	10.53 (82.11, −1.51)	403.57	10.53 (86.72, −1.59)	405.73	11.54 (119.91, −1.56)	
	213.21	−27.96 (−0.06, 0.55)	213.21	−28.86 (−0.07, 0.48)	213.21	−28.86 (−0.06, 0.47)	
	199.58	−22.18 (−0.05, 0.39)	200.01	−23.10 (−0.05, 0.74)	200.01	−23.09 (−0.05, 0.69)	
$(+\frac{3}{2})$	1276.28	111.60 (−0.11, −33.13)	1276.28	112.62 (−0.11, −35.00)	1290.75	115.45 (−0.11, −28.42)	
	943.34	122.24 (−0.18, 22.70)	943.34	124.17 (−0.20, 23.98)	943.34	126.99 (−0.19, 23.54)	
	405.73	19.24 (115.64, 4.52)	405.73	19.24 (122.13, 4.79)	405.73	19.24 (119.91, 4.70)	
	213.21	−27.96 (−0.06, −1.37)	213.21	−28.86 (−0.07, −1.45)	213.21	−28.86 (−0.06, −1.42)	
	200.90	−22.18 (−0.05, −2.36)	200.90	−23.09 (−0.05, −2.50)	200.45	−23.09 (−0.05, −2.25)	
$(-\frac{3}{2})$	1428.32	108.77 (−0.09, 16.18)	1451.06	109.68 (−0.09, 16.10)	1474.54	112.62 (−0.09, 14.67)	
	951.22	121.22 (−0.18, −22.19)	951.22	123.15 (−0.19, −23.54)	951.22	126.99 (−0.19, −23.01)	
	403.57	9.62 (82.11, −4.51)	403.57	9.62 (86.72, −4.75)	405.73	9.62 (119.91, −4.70)	
	213.21	−27.96 (−0.06, 1.37)	213.21	−28.86 (−0.07, 1.45)	213.21	−28.86 (−0.06, 1.42)	
	202.14	−23.09 (−0.05, 2.90)	202.14	−24.11 (−0.05, 3.06)	201.79	−24.11 (−0.05, 2.84)	

excitations in linear and nonlinear forms [50–56,58,70]. Relatively less significant dipole matrix elements are involved with the states $9P_{1/2,3/2}$ to $12P_{1/2,3/2}$ and $7F_{5/2,7/2}$ to $12F_{5/2,7/2}$ are evaluated using the second-order relativistic many-body perturbation theory [52]. The remaining matrix elements contribute little to the summations of Eq. (A1) to (A3) and are calculated using the Dirac-Fock method. Also, to achieve a better accuracy in the total dynamic polarizability values, we utilized the transition energies from the experimental data [71]. By employing the above methods, the static scalar polar-

izabilities $\alpha_V^0(0)$ of $5S_{\frac{1}{2}}$, $4D_{\frac{3}{2}}$, and $4D_{\frac{5}{2}}$ states are calculated as 87.68, 55.92, and 56.21 a.u., respectively, and static tensor polarizabilities $\alpha_V^2(0)$ of $4D_{\frac{3}{2}}$ and $4D_{\frac{5}{2}}$ states are computed as −34.67 and −47.12 a.u., respectively [17].

The core polarizability $\alpha^C(\omega)$ is valence-state-independent quantity and can be calculated quite accurately for a system having noble gas electronic configuration with core polarization corrected dipole matrix elements using third-order relativistic many-body perturbation theory [46,72]. Our calculation yields that the static core POL $\alpha^C(0)$ of the ion is

TABLE II. Magic wavelengths (in nm) with corresponding polarizabilities (in a.u.) of $^{87}\text{Sr}^+$ for different focusing angles of linearly polarized vortex beam with OAM = +1 for transitions $5S_{\frac{1}{2}}(+1/2) \rightarrow 4D_{\frac{3}{2}}(M_J)$. The values in the parentheses refer to vector polarizabilities at the corresponding magic wavelengths. In the parenthesis (a, b), “a” and “b” indicate the vector polarizabilities for $5S_{\frac{1}{2}}(+1/2)$ and $4D_{\frac{3}{2}}(M_J)$ states, respectively, in a.u.

State $4D_{\frac{3}{2}}(M_J)$	λ^{50°	α^{50°	λ^{60°	α^{60°	λ^{70°	α^{70°
OAM = +1						
$(+\frac{1}{2})$	1544.52	114.54 (−0.17, −4.39)	1523.86	116.47 (−0.18, −4.56)	1523.86	118.39 (−0.17, −4.31)
	1122.25	122.24 (−0.28, −5.30)	1122.25	124.17 (−0.28, −5.33)	1122.25	126.99 (−0.26, −5.46)
	403.57	18.22 (158.00, 2.14)	403.57	18.22 (156.69, 2.15)	403.57	18.22 (158.72, 2.03)
	212.22	−29.88 (−0.13, 1.44)	212.22	−29.88 (−0.13, 1.45)	212.22	−30.79 (−0.12, 1.36)
	202.14	−25.01 (−0.10, −0.89)	202.59	−26.03 (−0.10, −1.03)	202.14	−26.03 (−0.10, −0.91)
$(-\frac{1}{2})$	1656.85	113.53 (−0.16, 3.77)	1656.85	114.54 (−0.16, 3.78)	1627.26	117.37 (−0.15, 3.72)
	1122.25	122.24 (−0.28, 5.30)	1122.25	124.17 (−0.28, 5.33)	1122.25	126.99 (−0.26, 5.46)
	403.57	13.47 (158.00, −2.14)	403.57	13.47 (156.69, −2.15)	403.57	14.37 (158.72, −2.03)
	212.22	−29.88 (−0.13, −1.44)	212.22	−30.79 (−0.13, −1.45)	212.22	−30.79 (−0.12, −1.36)
	202.59	−25.01 (−0.10, 1.02)	202.59	−26.03 (−0.10, 1.03)	202.59	−26.94 (−0.10, 0.96)
$(+\frac{3}{2})$	1406.28	115.45 (−0.20, −18.64)	1428.32	117.37 (−0.20, −17.34)	1428.32	120.32 (−0.19, −16.37)
	1122.25	122.24 (−0.28, −15.94)	1122.25	124.17 (−0.28, −15.99)	1122.25	126.99 (−0.26, −15.09)
	403.57	23.09 (158.00, 6.52)	403.57	22.07 (156.69, 6.44)	403.57	22.07 (158.72, 6.10)
	212.22	−28.86 (−0.13, 4.33)	212.22	−30.79 (−0.13, 4.34)	212.22	−30.79 (−0.12, 4.10)
	201.79	−25.01 (−0.10, −2.68)	201.79	−25.01 (−0.10, −2.69)	201.79	−26.03 (−0.10, −2.56)
$(-\frac{3}{2})$	1712.91	112.62 (−0.15, 10.46)	1687.53	114.54 (−0.16, 10.86)	1687.53	117.37 (−0.15, 10.26)
	1122.25	122.24 (−0.28, 15.94)	1122.25	124.17 (−0.28, 15.99)	1122.25	126.99 (−0.26, 15.09)
	403.57	9.62 (158.00, −6.52)	403.57	9.62 (156.69, −6.44)	403.57	9.62 (158.72, −6.10)
	212.22	−29.88 (−0.13, −4.33)	212.22	−30.79 (−0.13, −4.34)	212.22	−30.79 (−0.12, −4.10)
	203.05	−26.03 (−0.10, 3.59)	203.50	−26.94 (−0.10, 4.04)	203.50	−26.94 (−0.10, 3.82)
$(+\frac{5}{2})$	1276.28	119.30 (−0.22, −46.32)	1276.28	120.32 (−0.22, −46.44)	1309.29	123.15 (−0.21, −36.17)
	1122.25	122.24 (−0.28, −26.57)	1122.25	124.17 (−0.28, −26.64)	1122.25	126.99 (−0.26, −25.16)
	403.57	26.93 (158.00, 10.70)	403.57	26.94 (156.69, 10.73)	403.57	26.94 (158.72, 10.15)
	212.22	−28.86 (−0.13, 7.23)	212.22	−30.79 (−0.13, 7.24)	212.22	−30.79 (−0.12, 6.84)
	201.79	−25.01 (−0.10, −4.48)	201.79	−26.03 (−0.10, −4.49)	201.79	−26.03 (−0.10, −4.24)
$(-\frac{5}{2})$	1687.53	112.62 (−0.16, 18.04)	1712.91	114.54 (−0.15, 17.48)	1712.91	117.37 (−0.14, 16.51)
	1122.25	122.24 (−0.28, 26.57)	1122.25	124.17 (−0.28, 26.64)	1122.25	126.99 (−0.26, 25.16)
	403.57	5.77 (158.00, −10.70)	403.57	5.77 (156.69, −10.73)	403.57	6.68 (158.72, −10.15)
	212.22	−29.88 (−0.13, −7.23)	212.22	−29.88 (−0.13, −7.24)	212.22	−30.79 (−0.12, −6.84)
	204.41	−26.03 (−0.10, 8.15)	203.95	−26.03 (−0.10, 7.46)	203.95	−26.93 (−0.10, 7.03)

6.103 a.u. The static core-valence parts $\alpha^{VC}(0)$ for the states $5S_{\frac{1}{2}}$, $4D_{\frac{3}{2}}$, and $4D_{\frac{5}{2}}$ are calculated to be -0.25 , -0.38 , and -0.42 a.u., respectively. All the magic and tune-out wavelengths calculated for the ion using the above-mentioned numerical procedure have maximum uncertainty of around $\pm 1\%$. To calculate the uncertainty, we replace the most important dipole matrix elements of the transitions: $5S_{\frac{1}{2}} \rightarrow 5P_{\frac{1}{2}, \frac{3}{2}}$ for $5S_{\frac{1}{2}}$, $4D_{\frac{3}{2}} \rightarrow 5P_{\frac{1}{2}, \frac{3}{2}}$, $4F_{\frac{5}{2}}$ for $4D_{\frac{3}{2}}$, and $4D_{\frac{5}{2}} \rightarrow 5P_{\frac{3}{2}, \frac{7}{2}}$ for $4D_{\frac{5}{2}}$ by the corresponding matrix elements calculated by Safronova [73] using single-double all-order method including partial triple excitations and recalculate the magic and tune-out wavelengths. The maximum difference between these recalculated wavelengths and the corresponding wavelengths obtained from our method gives the uncertainty of our results.

Calculation of the dynamic polarizability for ^{87}Rb

To determine the valence polarizability of the ground state $5S_{\frac{1}{2}}$ of ^{87}Rb at the hyperfine level, Eq. (A6) reduces to $\alpha_F^V(\omega) = C_0\alpha_{VF}^0(\omega) + C_1\alpha_{VF}^1(\omega)$. The tensor part of the po-

larizability is zero for the $5S_{\frac{1}{2}}$ state. Similar to the $^{87}\text{Sr}^+$ ion, here also, the dipole matrix elements involved with the states $5P_{1/2,3/2}$ to $8P_{1/2,3/2}$ and $9P_{1/2,3/2}$ to $12P_{1/2,3/2}$ are computed by using the relativistic coupled-cluster theory and second-order relativistic many-body perturbation theory, respectively. The $13P_{1/2,3/2}$ to $25P_{1/2,3/2}$ states and their associated matrix elements with the $5S_{\frac{1}{2}}$ state are calculated by using the Dirac-Fock method. To achieve better accuracy, the energy values of the states, used to calculate the polarizability values, are extracted from the experimental measurements [71]. For the $5S_{\frac{1}{2}}$ state of ^{87}Rb , we find that the static scalar, core, and core-valence polarizability values are 314.14, 9.11, and -0.26 a.u., respectively. The tune-out wavelengths of the hyperfine spin states of ^{87}Rb , discussed in the main text, have a maximum uncertainty of $\pm 0.1\%$.

Zeeman shift for ^{87}Rb and ^{23}Na

The Zeeman shifts for ^{87}Rb and ^{23}Na are evaluated by using $\hat{H}_Z = -\beta\hat{F}_Z + \gamma\hat{F}_Z^2$, where β and γ are the linear and quadratic Zeeman shifts, respectively. \hat{F}_Z represents the z

TABLE III. Magic wavelengths (in nm) with corresponding polarizabilities (in a.u.) of $^{87}\text{Sr}^+$ for different focusing angles of the linearly polarized vortex beam with $\text{OAM} = +2$ for transitions $5S_{\frac{1}{2}}(+1/2) \rightarrow 4D_{\frac{5}{2}}(M_J)$. The values in the parentheses refer vector polarizabilities at the corresponding magic wavelengths. In the parenthesis (a, b), “a” and “b” indicate the vector polarizabilities for $5S_{\frac{1}{2}}(+1/2)$ and $4D_{\frac{5}{2}}(M_J)$ states, respectively, in a.u.

State $4D_{\frac{5}{2}}(M_J)$	λ^{50°	α^{50°	λ^{60°	α^{60°	λ^{70°	α^{70°
OAM = +2						
$(+\frac{1}{2})$	2360.80	103.00 (−0.05, −0.93)	2149.21	105.83 (−0.05, −1.17)	2052.40	107.75 (−0.06, −1.25)
	1122.25	114.54 (−0.14, −2.61)	1122.25	116.47 (−0.14, −2.75)	1122.25	119.30 (−0.14, −2.70)
	405.73	14.37 (115.64, 1.05)	405.73	15.39 (122.13, 1.11)	405.73	15.39 (119.91, 1.09)
	212.22	−26.94 (−0.06, 0.71)	212.22	−27.96 (−0.07, 0.73)	212.22	−28.86 (−0.06, 0.73)
	201.34	−23.09 (−0.05, −0.40)	201.79	−23.09 (−0.05, −0.44)	201.34	−24.11 (−0.05, −0.42)
$(-\frac{1}{2})$	2489.80	103.00 (−0.05, 0.87)	2278.17	104.81 (−0.05, 1.05)	2149.21	107.75 (−0.06, 1.15)
	1122.25	114.54 (−0.14, 2.61)	1122.25	116.47 (−0.14, 2.75)	1122.25	119.30 (−0.14, 2.70)
	405.73	12.45 (115.64, −1.05)	403.57	13.24 (86.72, −1.11)	405.73	13.47 (119.91, −1.09)
	212.22	−26.94 (−0.06, −0.71)	212.02	−27.39 (−0.07, 2.09)	212.22	−28.86 (−0.06, −0.73)
	201.79	−23.09 (−0.05, 0.44)	201.88	−23.66 (−0.05, 0.44)	201.79	−24.11 (−0.05, 0.46)
$(+\frac{3}{2})$	1544.52	107.75 (−0.09, −6.45)	1544.52	108.77 (−0.09, −6.82)	1523.86	111.60 (−0.09, −6.93)
	1122.25	114.54 (−0.14, −7.81)	1122.25	116.47 (−0.14, −8.25)	1122.25	119.30 (−0.14, −8.10)
	405.73	18.22 (115.64, 3.15)	405.73	18.22 (122.13, 3.34)	405.73	18.22 (119.91, 3.27)
	212.22	−26.94 (−0.06, 2.13)	212.22	−27.96 (−0.07, 2.25)	212.22	−28.86 (−0.06, 2.20)
	201.79	−23.09 (−0.05, −1.31)	201.79	−23.09 (−0.05, −1.38)	201.79	−24.11 (−0.05, −1.37)
$(-\frac{3}{2})$	1752.44	105.83 (−0.07, 4.85)	1712.91	107.75 (−0.07, 5.41)	1712.91	109.68 (−0.07, 5.31)
	1122.25	114.54 (−0.14, 7.81)	1122.25	116.47 (−0.14, 8.25)	1122.25	119.30 (−0.14, 8.10)
	405.73	11.54 (115.64, −3.15)	403.57	11.54 (86.72, −3.34)	405.73	11.54 (119.91, −3.27)
	212.22	−26.94 (−0.06, −2.13)	212.22	−27.96 (−0.07, −2.25)	212.22	−28.86 (−0.06, −2.20)
	202.59	−23.09 (−0.05, 1.50)	202.59	−24.11 (−0.05, 1.59)	202.59	−24.11 (−0.05, 1.56)
$(+\frac{5}{2})$					1192.76	117.37 (−0.13, −37.85)
					1136.24	119.29 (−0.14, −41.59)
	405.73	22.07 (115.64, 5.25)	405.73	22.07 (122.13, 5.55)	405.73	22.07 (119.91, 5.45)
	212.22	−26.94 (−0.06, 3.54)	212.22	−27.96 (−0.07, 3.73)	212.22	−28.86 (−0.06, 3.67)
	203.05	−23.09 (−0.05, −2.72)	202.59	−24.11 (−0.05, −2.65)	202.59	−24.11 (−0.05, −2.60)
$(-\frac{5}{2})$	1276.28	110.70 (−0.11, 22.70)	1290.75	112.62 (−0.11, 21.72)	1328.38	114.54 (−0.11, 18.54)
	1122.25	114.54 (−0.14, 13.02)	1122.25	116.47 (−0.14, 13.74)	1122.25	119.30 (−0.14, 13.50)
	405.73	11.54 (115.64, −5.25)	403.57	11.54 (86.72, −5.55)	405.73	11.54 (119.91, −5.45)
	212.22	−26.94 (−0.06, −3.54)	212.22	−27.96 (−0.07, −3.73)	212.22	−28.86 (−0.06, −3.67)
	204.78	−24.11 (−0.05, 4.29)	204.41	−24.11 (−0.05, 4.23)	203.95	−25.01 (−0.05, 3.77)

component of the external magnetic field. The coefficients β and γ can be obtained from the power-series expansion of the Breit-Rabi formula [59]. The fine structure g_J and nuclear Landé g factors g_I , used in the Breit-Rabi formula, are 2.002 331 13 and $-0.000\,995\,141\,4$, respectively, for ^{87}Rb , while they are 2.00 229 60 and $-0.000\,804\,610$, respectively, for ^{23}Na [74]. Also, the ground-state hyperfine splittings of ^{87}Rb and ^{23}Na , required in the Breit-Rabi formula, have the values 6.8 and 1.7 GHz [74], respectively.

3. List of magic wavelengths with the corresponding vector and total polarizabilities

A list of magic wavelengths and the corresponding total polarizability values at these wavelengths for the transitions $5S_{\frac{1}{2}} \rightarrow 4D_{\frac{3}{2}, \frac{5}{2}}$ are presented in Tables I–III. Moreover, at each magic wavelength, values of the vector polarizabilities of the relevant states are quoted. Results are displayed for $\text{OAM} = +1$ and $+2$, while the focusing angles of the beam

are considered as 50° , 60° , and 70° . As seen in the tables, all the transitions between the magnetic sublevels of $5S_{\frac{1}{2}}$ and $4D_{\frac{3}{2}}$ and $4D_{\frac{5}{2}}$ states produce five sets of magic wavelengths except for a few cases, say, the $5S_{\frac{1}{2}} \rightarrow 4D_{\frac{5}{2}}$ transition for $\text{OAM} = +2$. Depending on the proximity of the resonances, the strength of the vector polarizability of one of the state dominates over the other state for a particular value of magic wavelength. For the $5S_{\frac{1}{2}} \rightarrow 4D_{\frac{5}{2}}(+5/2)$ transition, we have found (in Table III) that two sets of infrared magic wavelengths are missing at the focusing angles 50° and 60° of the beam, but all five sets of magic wavelengths are present at 70° , when the projected beam has $\text{OAM} = +2$. This highlights the direct effect of spin-orbit coupling of a linearly polarized vortex beam on the magic wavelengths. All the tables show that the magic wavelengths that fall in the visible and ultraviolet region of the electromagnetic spectrum support the blue-detuned trapping scheme confining the ion in the low-intensity region of the beam [75–78].

- [1] C. Champenois, M. Houssin, C. Lisowski, M. Knoop, G. Hagel, M. Vedel, and F. Vedel, *Phys. Lett. A* **331**, 298 (2004).
- [2] C. W. Chou, D. B. Hume, J. C. J. Koelemeij, D. J. Wineland, and T. Rosenband, *Phys. Rev. Lett.* **104**, 070802 (2010).
- [3] A. D. Ludlow, M. M. Boyd, J. Ye, E. Peik, and P. O. Schmidt, *Rev. Mod. Phys.* **87**, 637 (2015).
- [4] T. Lauprêtre, R. B. Linnet, I. D. Leroux, H. Landa, A. Dantan, and M. Drewsen, *Phys. Rev. A* **99**, 031401(R) (2019).
- [5] J. Schmidt, A. Lambrecht, P. Weckesser, M. Debatin, L. Karpa, and T. Schaetz, *Phys. Rev. X* **8**, 021028 (2018).
- [6] A. Lambrecht, J. Schmidt, P. Weckesser, M. Debatin, L. Karpa, and T. Schaetz, *Nat. Photon.* **11**, 704 (2017).
- [7] T. Schaetz, *J. Phys. B: At. Mol. Opt. Phys.* **50**, 102001 (2017).
- [8] G. W. Biedermann, X. Wu, L. Deslauriers, S. Roy, C. Mahadeswaraswamy, and M. A. Kasevich, *Phys. Rev. A* **91**, 033629 (2015).
- [9] H. S. Margolis, *J. Phys. B: At. Mol. Opt. Phys.* **42**, 154017 (2009).
- [10] P. Rosenbusch, S. Ghezali, V. A. Dzuba, V. V. Flambaum, K. Beloy, and A. Derevianko, *Phys. Rev. A* **79**, 013404 (2009).
- [11] T. Nicholson, S. Campbell, R. Hutson, G. Marti, B. Bloom, R. McNally, W. Zhang, M. Barrett, M. Safronova, G. Strouse *et al.*, *Nat. Commun.* **6**, 6896 (2015).
- [12] R. C. Dong, R. Wei, Y. B. Du, F. Zou, J. D. Lin, and Y. Z. Wang, *Appl. Phys. Lett.* **106**, 152402 (2015).
- [13] V. V. Flambaum, V. A. Dzuba, and A. Derevianko, *Phys. Rev. Lett.* **101**, 220801 (2008).
- [14] B. Arora, M. S. Safronova, and C. W. Clark, *Phys. Rev. A* **76**, 052509 (2007).
- [15] C. Lacroûte, K. S. Choi, A. Goban, D. J. Alton, D. Ding, N. P. Stern, and H. J. Kimble, *New J. Phys.* **14**, 023056 (2012).
- [16] B. Arora and B. K. Sahoo, *Phys. Rev. A* **86**, 033416 (2012).
- [17] A. Bhowmik, N. N. Dutta, and S. Majumder, *Phys. Rev. A* **97**, 022511 (2018).
- [18] A. Das, A. Bhowmik, N. N. Dutta, and S. Majumder, *Phys. Rev. A* **102**, 012801 (2020).
- [19] H. Kim, H. S. Han, and D. Cho, *Phys. Rev. Lett.* **111**, 243004 (2013).
- [20] L. Allen, M. W. Beijersbergen, R. J. C. Spreeuw, and J. P. Woerdman, *Phys. Rev. A* **45**, 8185 (1992).
- [21] M. Babiker, C. R. Bennett, D. L. Andrews, and L. C. Dávila Romero, *Phys. Rev. Lett.* **89**, 143601 (2002).
- [22] V. E. Lembessis, D. Ellinas, and M. Babiker, *Phys. Rev. A* **84**, 043422 (2011).
- [23] A. Afanasev, C. E. Carlson, and A. Mukherjee, *Phys. Rev. A* **88**, 033841 (2013).
- [24] P. K. Mondal, B. Deb, and S. Majumder, *Phys. Rev. A* **89**, 063418 (2014).
- [25] A. Bhowmik, P. K. Mondal, S. Majumder, and B. Deb, *Phys. Rev. A* **93**, 063852 (2016).
- [26] C. T. Schmiegelow, J. Schulz, H. Kaufmann, T. Ruster, U. G. Poschinger, and F. Schmidt-Kaler, *Nat. Commun.* **7**, 12998 (2016).
- [27] A. Bhowmik and S. Majumder, *J. Phys. Commun.* **2**, 125001 (2018).
- [28] J. Romero, D. Giovannini, S. Franke-Arnold, S. M. Barnett, and M. J. Padgett, *Phys. Rev. A* **86**, 012334 (2012).
- [29] S. Das, A. Bhowmik, K. Mukherjee, and S. Majumder, *J. Phys. B: At. Mol. Opt. Phys.* **53**, 025302 (2020).
- [30] G. F. Quinteiro, C. T. Schmiegelow, and F. Schmidt-Kaler, [arXiv:2004.00040](https://arxiv.org/abs/2004.00040).
- [31] F. L. Kien, P. Schneeweiss, and A. Rauschenbeute, *Eur. Phys. J. D* **67**, 92 (2013).
- [32] B. Albrecht, Y. Meng, C. Clausen, A. Dareau, P. Schneeweiss, and A. Rauschenbeutel, *Phys. Rev. A* **94**, 061401(R) (2016).
- [33] P. Schneeweiss, F. L. Kien, and A. Rauschenbeutel, *New J. Phys.* **16**, 013014 (2014).
- [34] J. Stenger, S. Inouye, D. M. Stampe-Kurn, H. J. Miesner, A. P. Chikkatur, and W. Ketterle, *Nature (London)* **396**, 345 (1998).
- [35] M.-S. Chang, C. D. Hamley, M. D. Barrett, J. A. Sauer, K. M. Fortier, W. Zhang, L. You, and M. S. Chapman, *Phys. Rev. Lett.* **92**, 140403 (2004).
- [36] M.-S. Chang, Q. S. Qin, W. X. Zhang, L. You, and M. S. Chapman, *Nat. Phys.* **1**, 111 (2005).
- [37] C. Klempt, O. Topic, G. Gebreyesus, M. Scherer, T. Henninger, P. Hyllus, W. Ertmer, L. Santos, and J. J. Arlt, *Phys. Rev. Lett.* **103**, 195302 (2009).
- [38] D. M. Stamper-Kurn and M. Ueda, *Rev. Mod. Phys.* **85**, 1191 (2013).
- [39] N. Akerman, N. Navon, S. Kotler, Y. Glickman, and R. Ozeri, *New J. Phys.* **17**, 113060 (2015).
- [40] Y. Shapira, R. Shaniv, T. Manovitz, N. Akerman, and R. Ozeri, *Phys. Rev. Lett.* **121**, 180502 (2018).
- [41] L. J. LeBlanc and J. H. Thywissen, *Phys. Rev. A* **75**, 053612 (2007).
- [42] X. Wang, J. Jiang, L.-Y. Xie, D.-H. Zhang, and C.-Z. Dong, *Phys. Rev. A* **94**, 052510 (2016).
- [43] J. Mitroy, M. S. Safronova, and C. W. Clark, *J. Phys. B: At. Mol. Opt. Phys.* **43**, 202001 (2010).
- [44] N. N. Dutta, S. Roy, and P. C. Deshmukh, *Phys. Rev. A* **92**, 052510 (2015).
- [45] T. K. Ghosh, A. K. Das, M. Castro, S. Canuto, and P. K. Mukherjee, *Phys. Rev. A* **48**, 2686 (1993).
- [46] N. N. Dutta, *Chem. Phys. Lett.* **758**, 137911 (2020).
- [47] B. Richards and E. Wolf, *Proc. R. Soc. London, Ser. A* **253**, 358 (1959).
- [48] A. Boivin and E. Wolf, *Phys. Rev.* **138**, B1561 (1965).
- [49] Y. Zhao, J. S. Edgar, G. D. M. Jeffries, D. McGloin, and D. T. Chiu, *Phys. Rev. Lett.* **99**, 073901 (2007).
- [50] I. Lindgren and J. Morrison, in *Atomic Many-Body Theory*, 3rd ed., edited by G. E. Lambropoulos and H. Walther (Springer, Berlin, 1985), Vol. 3.
- [51] R. F. Bishop and H. G. Kummel, *Phys. Today* **40**, 52 (1987).
- [52] I. Lindgren and J. Morrison, *Atomic Many-Body Theory* (Springer, Berlin, 1986).
- [53] I. Lindgren, *Phys. Rev. A* **31**, 1273 (1985).
- [54] R. J. Bartlett and M. Musial, *Rev. Mod. Phys.* **79**, 291 (2007).
- [55] N. N. Dutta and S. Majumder, *Indian J. Phys.* **90**, 373 (2016).
- [56] A. Bhowmik, S. Roy, N. N. Dutta, and S. Majumder, *J. Phys. B: At. Mol. Opt. Phys.* **50**, 125005 (2017).
- [57] A. Bhowmik, N. N. Dutta, and S. Roy, *Astrophys. J. Lett.* **836**, 125 (2017).
- [58] A. Das, A. Bhowmik, N. N. Dutta, and S. Majumder, *J. Phys. B: At. Mol. Opt. Phys.* **51**, 025001 (2018).
- [59] J. Vanier and C. Audoin, *The Quantum Physics of Atomic Frequency Standards* (Hilger, Philadelphia, 1988).
- [60] W. X. Zhang, D. L. Zhou, M. S. Chang, M. S. Chapman, and L. You, *Phys. Rev. A* **72**, 013602 (2005).

- [61] X. Li, B. Zhu, X. He, F. Wang, M. Guo, Z. F. Xu, S. Zhang, and D. Wang, *Phys. Rev. Lett.* **114**, 255301 (2015).
- [62] F. Fang, S. Wu, A. Smull, J. A. Isaacs, Y. Wang, C. H. Greene, and D. M. Stamper-Kurn, *Phys. Rev. A* **101**, 012703 (2020).
- [63] Q.-Q. Hu, C. Freier, Y. Sun, B. Leykauf, V. Schkolnik, J. Yang, M. Krutzik, and A. Peters, *Phys. Rev. A* **97**, 013424 (2018).
- [64] F. Schmidt, D. Mayer, M. Hohmann, T. Lausch, F. Kindermann, and A. Widera, *Phys. Rev. A* **93**, 022507 (2016).
- [65] R. Trubko, M. D. Gregoire, W. F. Holmgren, and A. D. Cronin, *Phys. Rev. A* **95**, 052507 (2017).
- [66] L. Li, B. Zhu, B. Lu, S. Zhang, and D. Wang, *Phys. Rev. A* **101**, 053611 (2020).
- [67] Y. Shi and Q. Niu, *Phys. Rev. Lett.* **96**, 140401 (2006).
- [68] K. Beloy, Ph.D. thesis, University of Nevada, Reno, 2009 (unpublished).
- [69] V. A. Dzuba, V. V. Flambaum, K. Beloy, and A. Derevianko, *Phys. Rev. A* **82**, 062513 (2010).
- [70] S. Biswas, A. Das, A. Bhowmik, and S. Majumder, *Mon. Not. R. Astron. Soc.* **477**, 5605 (2018).
- [71] A. Kramida, Y. Ralchenko, J. Reader, and NIST ASD Team (2019), NIST Atomic Spectra Database (ver. 5.7.1), <https://physics.nist.gov/asd> [2020, October 26].
- [72] W. R. Johnson, Z. W. Liu, and J. Sapirstein, *At. Data Nucl. Data Tables* **64**, 279 (1996).
- [73] U. I. Safronova, *Phys. Rev. A* **82**, 022504 (2010).
- [74] E. Arimondo, M. Inguscio, and P. Violino, *Rev. Mod. Phys.* **49**, 31 (1977).
- [75] S. A. Kennedy, G. W. Biedermann, J. T. Farrar, T. G. Akin, S. P. Krzyzewski, and E. R. I. Abraham, *Opt. Commun.* **321**, 110 (2014).
- [76] T. Kuga, Y. Torii, N. Shiokawa, T. Hirano, Y. Shimizu, and H. Sasada, *Phys. Rev. Lett.* **78**, 4713 (1997).
- [77] E. M. Wright, J. Arlt, and K. Dholakia, *Phys. Rev. A* **63**, 013608 (2000).
- [78] J. Arlt, K. Dholakia, and J. Soneson, *Phys. Rev. A* **63**, 063602 (2001).